Detailed dynamics modeling of BioBiped's monoarticular and biarticular tendon-driven actuation system

CONFERENCE PAPER *in* PROCEEDINGS OF THE ... IEEE/RSJ INTERNATIONAL CONFERENCE ON INTELLIGENT ROBOTS AND SYSTEMS. IEEE/RSJ INTERNATIONAL CONFERENCE ON INTELLIGENT ROBOTS AND SYSTEMS · JANUARY 2012

DOI: 10.1109/IROS.2012.6385564

3 AUTHORS:

Katayon Radkhah
Bosch GmbH
24 PUBLICATIONS **55** CITATIONS
SEE PROFILE

Thomas Lens
Technical University Darmstadt
13 PUBLICATIONS **56** CITATIONS
SEE PROFILE

Oskar Von Stryk
Technical University Darmstadt
184 PUBLICATIONS **1,588** CITATIONS
SEE PROFILE

Preprint of paper which appeared in the Proceedings of the 2012 IEEE/RSJ International Conference on Intelligent Robots and Systems, pp.4243-4250.

Detailed Dynamics Modeling of BioBiped's Monoarticular and Biarticular Tendon-Driven Actuation System

Katayon Radkhah, *Member*, *IEEE*, Thomas Lens, and Oskar von Stryk, *Member*, *IEEE*

***Abstract*— Bio-inspired, musculoskeletal design of bipedal robots offers great potential towards more human-like robot performance but imposes major challenges on their design and control, as it is challenging to analyze the contribution of each active and passive series elastic tendon to the overall joint, leg and robot dynamics. In this paper, detailed mathematical models of the tendon-driven, series elastically actuated mono- and biarticular structures of the BioBiped1 robot are presented. These enable a systematic analysis of the design space and characteristic curves as well as to derive guidelines for the design of improved prototypes. The derived models are applied to investigate the effects of the active and passive, mono- and biarticular structures on different performance criteria of 1D hopping motions by means of a detailed multi-body system dynamics simulation.**

I. INTRODUCTION

In the last decade compliant actuation has been identified as an important key towards natural motion performance [1]. It has been shown that elasticity in form of a spring can substantially reduce power and energy requirements demanded of an actuator. Inspired by the pioneering work of Pratt and Willamson [2], a series of cable- and tendon-based series elastic actuators (SEA) were developed and are used in finger systems [3], prostheses [4], exoskeletons [5], musculoskeletal upper torsos [6], and legged systems [7].

Steps towards human-like musculoskeletal robotic legs to replicate the muscle groups found in human legs were made in [8]–[10]. Hosoda et al. developed a pneumatically driven monopod with the main nine muscle groups involved in human locomotion (cf. Fig. 1(a)) to investigate biomechanical findings during jumping [8]. The robot Lucy was equipped with antagonist-agonist monoarticular muscle pairs to realize slow walking motions [9]. Niiyama et al. developed motor control for jumping and landing of a pneumatically actuated biped with biarticular muscles for jumping [10]. While, with respect to the long-term goal of energy-efficient and mobile bipedal robots, the use of pneumatics is not recommended, the integration of muscle-tendon structures seems to be a well supported idea by biomechanists. Monoarticular muscles in human legs spanning one joint are known to be essential for the power generation. Biarticular muscles passing over two joints transfer the power to the distal joint and synchronize the coordination of the coupled joints during dynamic jumping [11] and help to convert body segment rotations into desired translations of the body center of gravity [12]. In robotic systems biarticular structures and links have been integrated for varying purposes. Kino et al. studied in a detailed numerical approach the motion convergence of biarticular structures in a human-like modeled shoulder-elbow system to derive the system's behavior for specific desired equilibrium positions under zero-gravity conditions [13]. Lim et al. optimized a simulated rigid joint-link biped with one biarticular structure in the lower limb for jumping motions [14]. The common aim of these studies was a beneficial contribution of the used structures to the overall performance, in legged systems particularly for jumping motions up to now. However, emphasis did not lie on the development of mathematical models enabling a systematic analysis of the interactions of structures, actuators and joints by multi-body system (MBS) dynamics simulations at a high level of detail.

The BioBiped project aims at the realization of human-like jogging and walking abilities with musculoskeletal three-segmented legs using tendon-driven series elastic actuation. Energy-efficient actuation for dynamically locomoting bipedal robots is considered as a positive side effect of a well elaborated musculoskeletal system. It is explored whether human-like leg functions can be achieved by an intelligent coupling of control and actuation by harnessing the intrinsic passive dynamics of a properly designed musculoskeletal system. As for the actuation, the goal is not to develop new actuators, but to investigate the achievable locomotion performance by utilizing existing well established technologies in a bio-inspired setup to mimic muscle-tendon like structures: geared electric motors, extension springs and tendons. So far, two prototypes with three-segmented elastic legs, BioBiped1 (cf. Fig. 1(c)) and BioBiped2, have been built in this project by using different actuation concepts including mono- and biarticular structures. Both prototypes have rotational hip, knee and ankle joints and a simple trunk for stabilization purposes. At the current stage of the project the emphasis is set on the realization of human-like leg functionalities to realize fast dynamic hopping and jogging motions. To avoid interferences, the trunk of the BioBiped platforms are constrained to vertical (1D) or in-plane motions (2D). In experiments synchronous and alternate hopping motions with clear flight phases and ground clearances could be realized [15] (cf. videos [16]).

It is quite tedious, however, to systematically identify in experiments the role of the deployed tendon structures during the designed motion trajectories and the impact of their dynamics, e.g. joint torques, on the actuators. Such studies facilitate performance analyses with respect to design

This work was supported by the German Research Foundation (DFG) under grant no. STR 533/7-1. The authors gratefully acknowledge discussions on the musculoskeletal system with the BioBiped project members.

The authors are with the Simulation, Systems Optimization and Robotics Group, Technische Universität Darmstadt, 64289 Darmstadt, Germany. E-mail: radkhah@sim.tu-darmstadt.de

Preprint of paper which appeared in the Proceedings of the 2012 IEEE/RSJ International Conference on Intelligent Robots and Systems, pp.4243-4250.

modifications for future prototypes. Key to successful investigations is a mathematical modeling approach to capture the dynamics of the active and passive mono- and biarticular structures. However, a n dynamics model requires a much more complex MBS dynamics model than it is needed for conventional robots with rigid actuation.

The aim of this paper is to provide the working principles and models of the various actuation types integrated in the BioBiped robots. The models of the active/passive series elastic, mono- and biarticular actuation structures are studied in a detailed MBS dynamics simulation. The characteristic curves of motor and joint torques, as well as moment arms, are highly nonlinear depending on the coupled joint angle. In case of biarticular structures these curves vary based on two joint angles. For evaluation purpose of the presented actuator models we iteratively build up in simulation a detailed MBS dynamics model that finally includes seven muscle-tendon structures in each leg. To explore the effects of the structures, the simulation model is controlled to perform 1D hopping motions. Diagrams of the motor and joint dynamics including the torque amounts induced by each structure and ground reaction force patterns are used to derive insights and conclusions. As additional performance criterion we compute the energy consumed for each joint motion during all simulation runs.

The paper is organized as follows: In Section II we elucidate the mechanical design of BioBiped's actuation concept. In Section III detailed mathematical models are presented. Characteristic curves of a monoarticular structure are presented in Section IV. A simulation study for human-like hopping is described in Section V. Following a discussion in Section VI, the paper concludes with general remarks and future directions.

II. BioBiped's Actuation Concept

The actuation decisions for BioBiped1 are based on the involved muscle groups in human legs during dynamic motions, shown in Fig. 1(a) [17]. Accordingly, each joint has a pair of monoarticular antagonist-agonist muscles to flex and extend the connected limb: *Iliacus* (IL) - *Gluteus Maximus* (GL) in the hip, *Popliteus* (PL) - *Vastus lateralis* (VAS) in the knee and *Tibilias anterior* (TA) - *Soleus* (SOL) in the ankle joint. Additionally, three biarticular muscles transfer power from the knee to the hip or ankle joint, respectively: *Rectus femoris* (RF), *Biceps Femoris* (BF), and *Gastrocnemius* (GAS).

The actuators used are geared rotary electric direct-current motors (RE30 Maxon motors, 60 W, 24 V, with planetary reduction gearbox GP 32C with gear ratio 66:1). Each joint is actuated by one such unit; in total, six motors are used for both legs. In the following, we describe the technical realization of the structures illustrated in Fig. 1(b).

Hip actuation: As depicted in Fig. 2(a), the hip motor is connected via a timing belt to the joint. The transmission from motor to joint is not rigid due to small compression springs aligned in an inner ring around the joint. This *bidirectional SEA* (b-SEA) concept is similar to the original

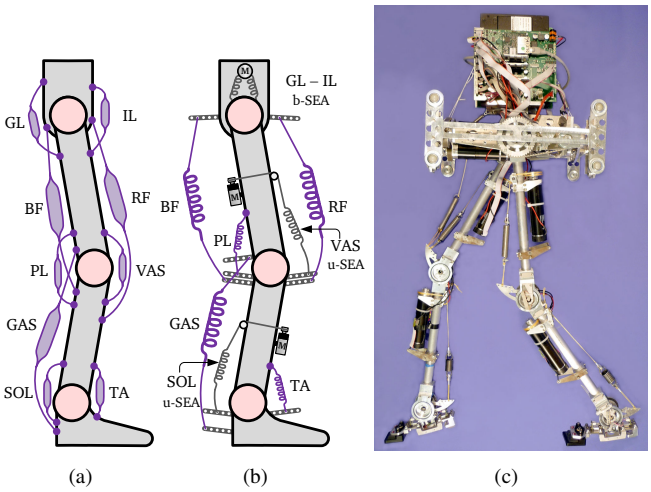

Fig. 1. Technical realization of BioBiped1's three-segmented leg actuation: (a) Main muscle groups in human legs. (b) Technical realization of the bi- and unidirectional elastic structures in the legs of BioBiped1. The passive structures in purple are detachable. (c) Real BioBiped1 platform.

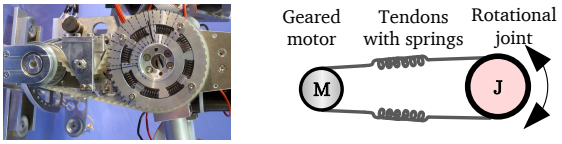

Fig. 2. Construction (a) and drawing (b) of the bidirectional hip actuation.

SEA [2] introducing elasticity directly in the joint. The b-SEA represents the muscle pair IL - GL.

Knee and ankle actuation: The knee and ankle joints are each actuated by a combination of a *unidirectional SEA* (u-SEA) and its passive counterpart. Each joint is actively extended by an elastic tendon, consisting of the motor connected to the joint via a Dyneema tendon with built-in extension spring. As illustrated in Fig. 3(b), the motor adjusts the equilibrium length of the elastic tendon by winding the tendon around the pulley that is attached to the motor axle. On the joint side five different force application points can be chosen to attach the tendon to the joint (cf. Fig. 3(c)). This actuation concept introduces varying lever arms and transmission ratios aside from highly nonlinear joint torques and stiffnesses. Both, the VAS and SOL muscle, are represented by a u-SEA. The flexing muscles in knee and ankle joint, PL and TA, can be integrated as passive structures by a Dyneema tendon with built-in extension spring, referred to as *monoarticular, passive structure*. Different attachment points can be selected to attach the tendon to the joint.

The biarticular muscles, RF, BF, and GAS, are realized in the same way as the passive structures PL and TA, with the difference that they connect two segments. Here again, the construction permits different fixation points and springs to be chosen as well. These structures represent the group of *biarticular, passive structures*. Note that only the actuated muscle groups, IL - GL, VAS and SOL, are always integrated in BioBiped1. Depending on a motion a passive structure can be detached and attached as desired. This allows a better synthesis as described in Section V.

Preprint of paper which appeared in the Proceedings of the 2012 IEEE/RSJ International Conference on Intelligent Robots and Systems, pp.4243-4250.

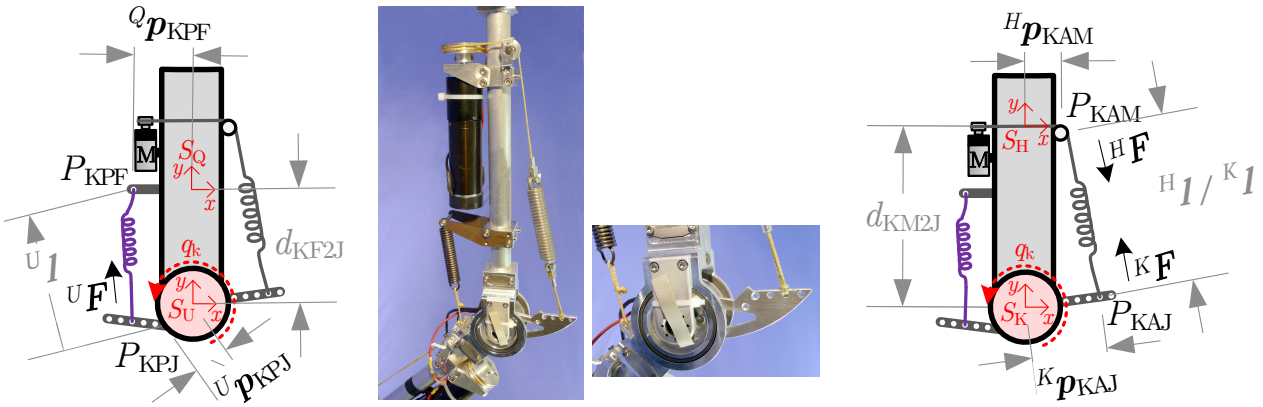

(a) (b) (c) (d)

Fig. 3. Construction (b) of the knee actuation with (c) a close-up of the attachment mechanism. The distance of the five attachment points from the knee joint vary between 36.4 for the nearest and 66.5 mm for the farthest fixation point. A schematic drawing of the PL structure for the flexion of the knee joint is depicted in (a). The drawing of the active counterpart, VAS, is shown in (d).

The robot is about 1.1 m tall in extended position and weighs around 10 kg. The segment lengths are based on scaled-down anthropometric data. For details on segment masses and foot dimensions we refer to [15] and the accompanying video.

III. Detailed Physical Modeling

In this section we focus on modeling of the elastic transmissions of the four actuator types: (1) monoarticular, b-SEA, (2) monoarticular, u-SEA, (3) monoarticular, passive structure, and (4) biarticular, passive structure. The model of the motor electrical dynamics is described as:

$$u = R_{\mathrm{a}}\, i + k_{\mathrm{v}}\, \dot{\theta} = \frac{R_{\mathrm{a}}}{k_{\mathrm{t}}}\, \tau_{\mathrm{m}} + k_{\mathrm{v}}\, \dot{\theta} \tag{1}$$

with motor angular velocity $\dot{\theta}$, input voltage u, armature resistance R_{a}, torque constant k_{t}, speed constant k_{v} and generated motor torque τ_{m}, which drives the rotor. The effect of armature inductance is neglected. The mechanical dynamics of the motor is formulated as:

$$I_{\mathrm{m}}\, \ddot{\theta} + d_{\mathrm{m}}\, \dot{\theta} = \tau_{\mathrm{m}} - \mu\, \tau_{\mathrm{e,M}} \tag{2}$$

with motor inertia I_{m}, damping d_{m} and μ gearbox efficiency. $\tau_{\mathrm{e,M}}$ is the elastic torque induced through the transmission on the motor. All variables and parameters are reflected to the joint side by a total ratio caused by the gear and elastic tendon transmission.

A. Monoarticular b-SEA

From the utilized actuators, the b-SEA represents the simplest actuation concept describing a linear transmission relation. The torque transmitted to the joint/link through the elastic spring of constant torsional stiffness k and damping d_{e} is:

$$\tau_{\mathrm{e,J}} = k\, (\theta - q) + d_{\mathrm{e}}\, (\dot{\theta} - \dot{q})\,, \tag{3}$$

with q and θ denoting the measured joint and motor position. Note that the same torque is also exerted on the motor for this special case of transmission: $\tau_{\mathrm{e,M}} = \tau_{\mathrm{e,J}}$ holds for reflected variables. For future reference we denote $\tau_{\mathrm{e,J}}$ as τ_{GLIL}.

B. Monoarticular u-SEA

A schematic drawing of this actuation concept is shown in Fig. 3(d) for the knee. In contrast to the b-SEA, here we have a strong nonlinear coupling of joint with the motor. The transmission creates different torques on the joint and motor. Transmission ratio, lever arms and output stiffnesses nonlinearly change during joint movement. For the formulation of the equations we locate coordinate reference frames on the thigh segment at the height of the pulley and directly in the knee joint, S_H and S_K. We make the assumption that the origin of the frames, tendon, and attachment points span exactly one plane such that the third dimension of each vector $\in \mathbf{R}^3$ in the following equations is set to zero. The definitions of points assigned to the actuation mechanism are provided in Table I.

To compute the motor and joint torques, we first calculate the extension of the built-in spring. The elongation depends on the amount of tendon wrapped on the gearbox shaft and on the joint state. At the rest angle q_0 the tendon is at rest. Neglecting the deformation of the tendon, we can formulate any change in the spring as follows:

$$\Delta l(q,\theta) = \left\|{}^{K}\boldsymbol{l}(q)\right\| - \left\|{}^{K}\boldsymbol{l}(q_0)\right\| + |\theta|\; r_{\mathrm{M}}\,, \tag{4}$$

with r_{M} denoting the radius of the gearhead output shaft. The exact definition of ${}^{K}\boldsymbol{l}$ is provided in Table I.

At $q = q_0$ and $\theta = 0$ tendon forces ${}^{K}\boldsymbol{F}$ are equal to zero. Slacking of the tendon is not considered:

$${}^{K}\boldsymbol{F}(q,\theta) = \begin{cases} k\, \Delta l(q,\theta)\, \frac{{}^{K}\boldsymbol{l}(q)}{\|{}^{K}\boldsymbol{l}(q)\|} & \text{for } \Delta l(q,\theta) > 0 \\ 0 & \text{for } \Delta l(q,\theta) \leq 0 \end{cases} \tag{5}$$

k stands for the constant spring stiffness. The torque exerted on the joint by the spring elongation can now be defined as the following cross and dot product:

$$\begin{aligned} {}^{K}\boldsymbol{\tau}(q,\theta) &= {}^{K}\boldsymbol{p}_{\mathrm{KAJ}} \times {}^{K}\boldsymbol{F}(q,\theta) \\ &= \boldsymbol{p}_{\mathrm{lever}}(q) \times {}^{K}\boldsymbol{F}(q,\theta)\,, \end{aligned} \tag{6}$$

$$\tau_{\mathrm{e,J}}(q,\theta) = {}^{K}\boldsymbol{\tau}(q,\theta) \bullet e_Z\,. \tag{7}$$

Preprint of paper which appeared in the Proceedings of the 2012 IEEE/RSJ International Conference on Intelligent Robots and Systems, pp.4243-4250.

TABLE I
DEFINITIONS FOR THE U-SEA VAS

${}^{H}\boldsymbol{R}_{K}(q)$	$= \mathrm{Rot}_z(q)$
$\mathrm{Rot}_z(q)$	Elementary rotation around the z-axis about an angle q $= \begin{pmatrix} \cos q & -\sin q & 0 \\ \sin q & \cos q & 0 \\ 0 & 0 & 1 \end{pmatrix}$
${}^{H}\boldsymbol{r}_{K}$	Translation vector from the origin of S_H to the origin of S_K: $= \begin{pmatrix} 0 \\ -d_{\mathrm{KM2J}} \\ 0 \end{pmatrix}$
${}^{H}\boldsymbol{p}_{\mathrm{KAM}}$	Constant distance vector of the fixed point P_{KAM} from the origin of S_H
${}^{K}\boldsymbol{p}_{\mathrm{KAJ}}$	Constant distance vector of the moving tendon fixation point P_{KAJ} from the origin of S_K
${}^{H}\boldsymbol{p}_{\mathrm{KAJ}}(q)$	$= {}^{H}\boldsymbol{r}_{K} + {}^{H}\boldsymbol{R}_{K}(q)\,{}^{K}\boldsymbol{p}_{\mathrm{KAJ}}$
${}^{K}\boldsymbol{p}_{\mathrm{KAM}}(q)$	$= {}^{K}\boldsymbol{r}_{H}(q) + {}^{K}\boldsymbol{R}_{H}(q)\,{}^{H}\boldsymbol{p}_{\mathrm{KAM}}$
${}^{K}\boldsymbol{l}(q)$	length vector of the tendon in S_K $= {}^{K}\boldsymbol{p}_{\mathrm{KAM}}(q) - {}^{K}\boldsymbol{p}_{\mathrm{KAJ}}$
${}^{H}\boldsymbol{l}(q)$	length vector of the tendon in S_H $= {}^{H}\boldsymbol{p}_{\mathrm{KAJ}}(q) - {}^{H}\boldsymbol{p}_{\mathrm{KAM}}$

For clarity, we refer to $\tau_{\mathrm{e,J}}$ as τ_{VAS}. The nonlinearly changing lever arm only depends on q and is computed as follows:

$$\boldsymbol{p}_{\mathrm{lever}}(q) = {}^{K}\boldsymbol{p}_{\mathrm{KAJ}} - \frac{{}^{K}\boldsymbol{p}_{\mathrm{KAJ}} \bullet {}^{K}\boldsymbol{l}(q)}{\left\|{}^{K}\boldsymbol{l}(q)\right\|^2}\,{}^{K}\boldsymbol{l}(q) \tag{8}$$

Depending on motor and joint state which is additionally affected by gravitational and antagonistic forces, τ_{VAS} can be both either positive or negative (cf. positive rotation direction of S_K in Fig. 3(d)).

The computation of the motor torques caused by the spring elongation follows the same approach as in (4) - (5):

$${}^{H}\boldsymbol{F}(q,\theta) = \begin{cases} k\,\Delta l(q,\theta)\,\frac{{}^{H}\boldsymbol{l}(q)}{\|{}^{H}\boldsymbol{l}(q)\|} & \text{for } \Delta l(q,\theta) > 0 \\ 0 & \text{for } \Delta l(q,\theta) \le 0 \end{cases} \tag{9}$$

An important difference is that, in contrast to the moving attachment point P_{KAJ}, the point P_{KAM} is fixed. Thus, the cross product can be simplified to:

$$\tau_{\mathrm{e,M}}(q,\theta) = -r_{\mathrm{M}}\,\left\|{}^{H}\boldsymbol{F}(q,\theta)\right\| . \tag{10}$$

In contrast to a b-SEA, here $\tau_{\mathrm{e,J}} \neq \tau_{\mathrm{e,M}}$ holds in general. Equations (4)-(10) are also applicable to the u-SEA in the ankle to compute the motor torques, lever arms and joint torques τ_{SOL}.

C. Monoarticular passive structure

The equations for a monoarticular, passive structure can be set up in a similar way. As soon as the VAS structure is extended, the PL structure will induce a negative torque on the knee at a specific time instant depending on the set rest length q_0. Here, the spring elongation only depends on the coupled joint angle q. Therefore, (4) is reduced to:

$$\Delta l(q) = \left\|{}^{U}\boldsymbol{l}(q)\right\| - \left\|{}^{U}\boldsymbol{l}(q_0)\right\| , \tag{11}$$

to compute the spring elongation of the PL structure with ${}^{U}\boldsymbol{l}$ denoting the length vector in the S_U frame, as depicted in Fig. 3(a). Subsequently, the computation of the force vector,${}^{U}\boldsymbol{F}$, and torque generated by PL on the knee joint, τ_{PL}, can be carried out according to (5)-(7). The same procedure also applies to the passive TA tendon to determine τ_{TA} on the ankle joint.

TABLE II
DEFINITIONS FOR THE BIARTICULAR, PASSIVE STRUCTURE GAS

${}^{\mathrm{Kne}}\boldsymbol{T}_{\mathrm{Ank}}(q_{\mathrm{k}},q_{\mathrm{a}})$	$= \begin{pmatrix} \mathrm{Rot}_z(q_{\mathrm{k}}+q_{\mathrm{a}}) & \mathrm{Rot}_z(q_{\mathrm{k}})\,{}^{\mathrm{Kne}}\boldsymbol{r}_{\mathrm{Ank}} \\ 0 & 1 \end{pmatrix}$
${}^{\mathrm{Ank}}\boldsymbol{T}_{\mathrm{Kne}}(q_{\mathrm{a}},q_{\mathrm{k}})$	$= \begin{pmatrix} \mathrm{Rot}_z(q_{\mathrm{k}}+q_{\mathrm{a}})^T & -\mathrm{Rot}_z(q_{\mathrm{a}})^T\,{}^{\mathrm{Kne}}\boldsymbol{r}_{\mathrm{Ank}} \\ 0 & 1 \end{pmatrix}$
${}^{\mathrm{Kne}}\boldsymbol{p}_{\mathrm{GK}}$	Constant distance vector of the moving tendon fixation point P_{GK} relative to the origin of S_{Kne}
${}^{\mathrm{Ank}}\boldsymbol{p}_{\mathrm{GA}}$	Constant distance vector of the moving tendon fixation point P_{GA} relative to the origin of S_{Ank}
${}^{\mathrm{Kne}}\boldsymbol{l}(q_{\mathrm{k}},q_{\mathrm{a}})$	$= {}^{\mathrm{Kne}}\boldsymbol{p}_{\mathrm{GA}}(q_{\mathrm{k}},q_{\mathrm{a}}) - {}^{\mathrm{Kne}}\boldsymbol{p}_{\mathrm{GK}}$
${}^{\mathrm{Ank}}\boldsymbol{l}(q_{\mathrm{a}},q_{\mathrm{k}})$	$= {}^{\mathrm{Ank}}\boldsymbol{p}_{\mathrm{GK}}(q_{\mathrm{a}},q_{\mathrm{k}}) - {}^{\mathrm{Ank}}\boldsymbol{p}_{\mathrm{GA}}$
$\Delta l(q_{\mathrm{k}},q_{\mathrm{a}})$	$= \left\|{}^{\mathrm{Kne}}\boldsymbol{l}(q_{\mathrm{k}},q_{\mathrm{a}})\right\| - \left\|{}^{\mathrm{Kne}}\boldsymbol{l}(q_{\mathrm{k0}},q_{\mathrm{a0}})\right\|$ with q_{a0} and q_{k0} denoting the rest angles in ankle and knee joint

D. Biarticular passive structure

A distinctive feature of biarticular structures is that their dynamics affect simultaneously two joints. In the following, a sample calculation is performed for the GAS structure (cf. Fig. 4) applying the virtual work and displacement method from above. First, it is essential to capture the orientation and position of the used reference frames S_{Kne} and S_{Ank} w.r.t each other, as given in Table II. Both frames are directly located on the joint axles. Subsequently, we can express the moving tendon fixation points P_{GA} and P_{GK} relative to these frames as follows:

$${}^{\mathrm{Kne}}\boldsymbol{p}_{\mathrm{GA}}(q_{\mathrm{k}},q_{\mathrm{a}}) = {}^{\mathrm{Kne}}\boldsymbol{T}_{\mathrm{Ank}}(q_{\mathrm{k}},q_{\mathrm{a}})\,{}^{\mathrm{Ank}}\boldsymbol{p}_{\mathrm{GA}} , \tag{12}$$

$${}^{\mathrm{Ank}}\boldsymbol{p}_{\mathrm{GK}}(q_{\mathrm{a}},q_{\mathrm{k}}) = {}^{\mathrm{Ank}}\boldsymbol{T}_{\mathrm{Kne}}(q_{\mathrm{a}},q_{\mathrm{k}})\,{}^{\mathrm{Kne}}\boldsymbol{p}_{\mathrm{GK}} . \tag{13}$$

q_{a} and q_{k} denote the ankle and knee angles. Provided that the spring is extended, i.e. $\Delta l(q_{\mathrm{a}},q_{\mathrm{k}}) > 0$, the occurring tendon forces are computed, similar to (5) and (9):

$${}^{\mathrm{Kne}}\boldsymbol{F}(q_{\mathrm{k}},q_{\mathrm{a}}) = k\,\Delta l(q_{\mathrm{k}},q_{\mathrm{a}})\,\frac{{}^{\mathrm{Kne}}\boldsymbol{l}(q_{\mathrm{k}},q_{\mathrm{a}})}{\|{}^{\mathrm{Kne}}\boldsymbol{l}(q_{\mathrm{k}},q_{\mathrm{a}})\|} \tag{14}$$

$${}^{\mathrm{Ank}}\boldsymbol{F}(q_{\mathrm{a}},q_{\mathrm{k}}) = k\,\Delta l(q_{\mathrm{a}},q_{\mathrm{k}})\,\frac{{}^{\mathrm{Ank}}\boldsymbol{l}(q_{\mathrm{a}},q_{\mathrm{k}})}{\|{}^{\mathrm{Ank}}\boldsymbol{l}(q_{\mathrm{a}},q_{\mathrm{k}})\|} \tag{15}$$

The cross product is applied to retrieve the torques at knee and ankle joint produced by the GAS structure:

$${}^{\mathrm{Kne}}\boldsymbol{\tau}(q_{\mathrm{k}},q_{\mathrm{a}}) = {}^{\mathrm{Kne}}\boldsymbol{p}_{\mathrm{GK}} \times {}^{\mathrm{Kne}}\boldsymbol{F}(q_{\mathrm{k}},q_{\mathrm{a}}) \tag{16}$$

$${}^{\mathrm{Ank}}\boldsymbol{\tau}(q_{\mathrm{a}},q_{\mathrm{k}}) = {}^{\mathrm{Ank}}\boldsymbol{p}_{\mathrm{GA}} \times {}^{\mathrm{Ank}}\boldsymbol{F}(q_{\mathrm{a}},q_{\mathrm{k}}) \tag{17}$$

As in (6) ${}^{\mathrm{Kne}}\boldsymbol{p}_{\mathrm{GK}}$ and ${}^{\mathrm{Ank}}\boldsymbol{p}_{\mathrm{GA}}$ are both exchangeable with the corresponding moment arm vectors, for which (8) is applicable. To summarize, the torque amount induced by the GAS structure on the knee joint is:

$$\tau_{\mathrm{GAS,Kne}}(q_{\mathrm{k}},q_{\mathrm{a}}) = {}^{\mathrm{Kne}}\boldsymbol{\tau}(q_{\mathrm{k}},q_{\mathrm{a}}) \bullet e_Z , \tag{18}$$

Preprint of paper which appeared in the Proceedings of the 2012 IEEE/RSJ International Conference on Intelligent Robots and Systems, pp.4243-4250.

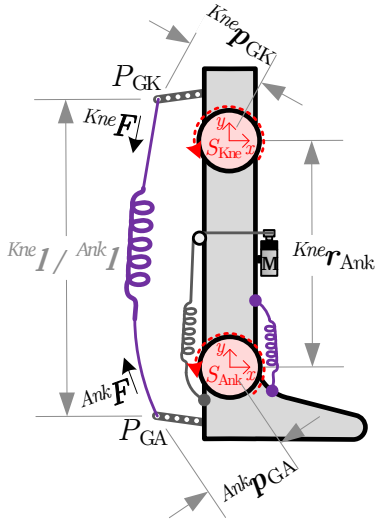

Fig. 4. Schematic drawing of the GAS structure on the left.

respectively on the ankle joint:

$$\tau_{\mathrm{GAS,Ank}}(q_{\mathrm{a}}, q_{\mathrm{k}}) = {}^{\mathrm{Ank}}\boldsymbol{\tau}(q_{\mathrm{a}}, q_{\mathrm{k}}) \bullet e_Z \,. \tag{19}$$

The same procedure can be applied to compute the torque amount by the BF structure induced on the hip and knee joint, denoted as $\tau_{\mathrm{BF,Hip}}$ and $\tau_{\mathrm{BF,Kne}}$, and by RF exerted also at hip and knee joint, referred to as $\tau_{\mathrm{RF,Hip}}$ and $\tau_{\mathrm{RF,Kne}}$.

IV. Characteristic Curves

Now that the torque amounts caused by all actuator types are known, we can formulate the general output torque functions for each joint. Let us introduce the following notations for joint torques generated by a b-SEA τ_{bsea}, u-SEA τ_{usea}, monoarticular passive structure τ_{mono} and biarticular passive structure τ_{bi}. Then, the general output torque function for the knee and ankle joint can be written as:

$$\tau_{\mathrm{e,J}}(q, \theta, q_2) = \tau_{\mathrm{usea}}(q, \theta) + \tau_{\mathrm{mono}}(q) + \tau_{\mathrm{bi}}(q, q_2) \,, \tag{20}$$

with q_2 denoting the angle of the second joint coupled by the biarticular structure. The function for the hip joint is:

$$\tau_{\mathrm{e,J}}(q, \theta, q_2) = \tau_{\mathrm{bsea}}(q, \theta) + \tau_{\mathrm{bi}}(q, q_2) \,, \tag{21}$$

where τ_{bsea} is replaced by the result of (3). Deriving (20) and (21) w. r. t. θ, q and q_2 yields the output stiffness functions:

$$\frac{\mathrm{d}\tau_{\mathrm{usea}}}{\mathrm{d}\theta} + \frac{\mathrm{d}\tau_{\mathrm{usea}}}{\mathrm{d}q} + \frac{\mathrm{d}\tau_{\mathrm{mono}}}{\mathrm{d}q} + \frac{\mathrm{d}\tau_{\mathrm{bi}}}{\mathrm{d}q} + \frac{\mathrm{d}\tau_{\mathrm{bi}}}{\mathrm{d}q_2} \tag{22}$$

respectively

$$\frac{\mathrm{d}\tau_{\mathrm{bsea}}}{\mathrm{d}\theta} + \frac{\mathrm{d}\tau_{\mathrm{bsea}}}{\mathrm{d}q} + \frac{\mathrm{d}\tau_{\mathrm{bi}}}{\mathrm{d}q} + \frac{\mathrm{d}\tau_{\mathrm{bi}}}{\mathrm{d}q_2} \tag{23}$$

While the number of b-SEAs, u-SEAs and monoarticular, passive structures is restricted to one per leg joint, the number of biarticular structures can be up to three. The exact output torque functions for all leg joints, considering all structures in Fig. 1(b), are given in (24) - (26). Obviously, the describing output equations can become quite complex. These output functions are highly nonlinear and depend on several parameters. To give an idea of the complexity of the design space, we investigate the dynamics caused only by the VAS structure with stiffness 15k N/m, neglecting all passive torque amounts in (25). The diagrams in Fig. 5 display the motor and joint torques in the workspace $\theta = [0, 90°]$ and $q = [-90°, 0]$ at rest angle $q_0 = -90°$, corresponding to a bent knee, for attachment point number 5 (cf. Fig. 3(c)). At the end position of the q-interval, $q = 0°$, the knee is completely extended. The curves illustrate the nonlinear dependency of the joint and motor torques on the joint movement. Also, the curves are different for varying attachment points, as shown in Fig. 6. Even with an incomplete joint torque function for the knee joint considering only one structure, the dimension of the design space with its many key parameters appear as quite large. Due to the complexity behavior predictions for a joint, when all structures are included, are difficult. Only with regard to the antagonistic muscles it is clear that for instance the co-contraction of PL, which introduces opposing torques on the motor, makes the knee stiffer. The same holds true for the muscle pair in the ankle. For general statements, however, a sophisticated framework is required that allows to analyze the effects of variations in spring stiffnesses, attachment points, and rest lengths on the overall joint behavior with respect to well chosen gait-specific performance criteria.

V. Application and Evaluation

As application and evaluation of the above introduced mathematical models detailed MBS dynamics simulations are performed for different configurations of the compliant actuation of the leg for the case of hopping on the spot to investigate their effect on different performance criteria. The motor trajectories and control are not changed such that the reason for any observed effects and changes can be clearly identified. For the simulations we use a self-developed simulation toolbox in Matlab/Simulink [18]. Details of the MBS dynamics model of the rigid joint-link structure and the experimentally validated ground contact model can be found in [18]. As the focus is set solely on the realization of a proper leg function for hopping, the trunk of the robot model is restricted to vertical 1D motion. The accompanying video contains animations of the motion dynamics simulations of the robot model and diagrams illustrating the course of all motor and joint states. The diagrams also include the voltage trajectories to ensure that the voltage limitations of ±24 V are not violated. Ground contact dynamics are depicted as well, where applicable. The overall evaluation of the simulation runs is additionally supported by the consumed energy which is an important criterion for human-like performance. The following formula is used to determine the power:

$$\begin{aligned} P(t) &= \left(\frac{R_{\mathrm{a}}}{k_{\mathrm{t}}} \cdot \tau_{\mathrm{m}} + k_{\mathrm{v}} \dot{\theta} \right) \cdot \frac{\tau_{\mathrm{m}}}{k_{\mathrm{t}}} \\ &= \left(\frac{R_{\mathrm{a}}}{k_{\mathrm{t}}^2} \cdot \tau_{\mathrm{m}}^2 + \frac{k_{\mathrm{v}}}{k_{\mathrm{t}}} \cdot \dot{\theta} \cdot \tau_{\mathrm{m}} \right) \,. \end{aligned} \tag{27}$$

The current BioBiped1 hardware platform uses external power supply and does not have energy recovery mecha-

$$\tau_{\mathrm{e,Hip}}(q_{\mathrm{Hip}}, \theta_{\mathrm{Hip}}, q_{\mathrm{Kne}}) = \tau_{\mathrm{GLIL}}(q_{\mathrm{Hip}}, \theta_{\mathrm{Hip}}) + \tau_{\mathrm{RF,Hip}}(q_{\mathrm{Hip}}, q_{\mathrm{Kne}}) + \tau_{\mathrm{BF,Hip}}(q_{\mathrm{Hip}}, q_{\mathrm{Kne}}) \tag{24}$$

$$\tau_{\mathrm{e,Kne}}(q_{\mathrm{Kne}}, \theta_{\mathrm{Kne}}, q_{\mathrm{Ank}}) = \tau_{\mathrm{VAS}}(q_{\mathrm{Kne}}, \theta_{\mathrm{Kne}}) + \tau_{\mathrm{PL}}(q_{\mathrm{Kne}}) + \tau_{\mathrm{GAS,Kne}}(q_{\mathrm{Kne}}, q_{\mathrm{Ank}}) + \tau_{\mathrm{RF,Kne}}(q_{\mathrm{Kne}}, q_{\mathrm{Hip}}) + \tau_{\mathrm{BF,Kne}}(q_{\mathrm{Kne}}, q_{\mathrm{Hip}}) \tag{25}$$

$$\tau_{\mathrm{e,Ank}}(q_{\mathrm{Ank}}, \theta_{\mathrm{Ank}}, q_{\mathrm{Kne}}) = \tau_{\mathrm{SOL}}(q_{\mathrm{Ank}}, \theta_{\mathrm{Ank}}) + \tau_{\mathrm{TA}}(q_{\mathrm{Ank}}) + \tau_{\mathrm{GAS,Ank}}(q_{\mathrm{Ank}}, q_{\mathrm{Kne}}) \tag{26}$$

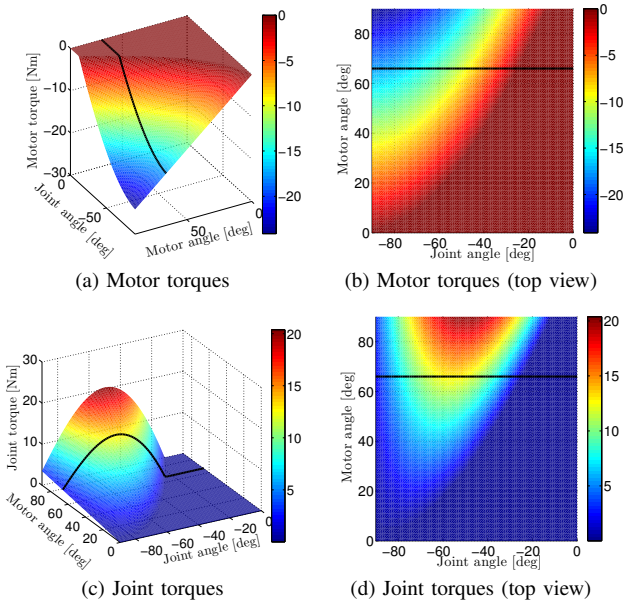

(a) Motor torques (b) Motor torques (top view)

(c) Joint torques (d) Joint torques (top view)

Fig. 5. Motor torques induced by the monoarticular u-SEA VAS in the view from the front (a) and from the top (b) for $q_0 = -90°$, $\theta = [0, 90°]$, $q = [-90°, 0]$ and attachment point number 5 (AP 5). Joint torques generated by VAS for the same setting in the front view (c) and top view (d). The black line represents the curves at motor angle $\theta = 66°$ (cf. Fig. 6). In flat areas slacking of the tendon occurs.

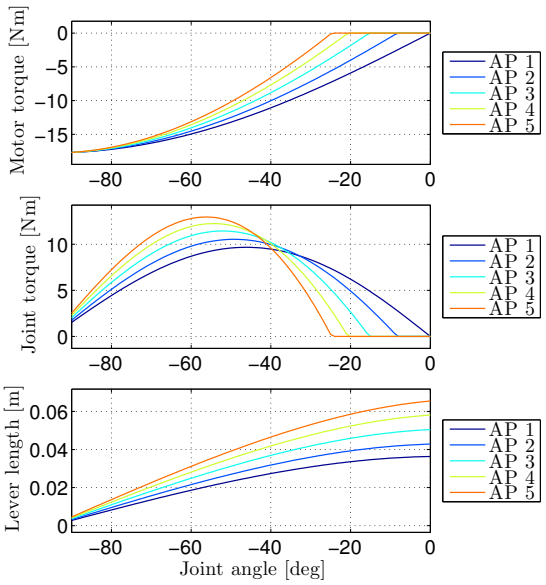

Fig. 6. Motor torques, joint torques and lever lengths for the same settings as in Fig. 5 for all attachment points, abbreviated as AP in the legends above, when the motor is fixed at $\theta = 66°$. The black line in all diagrams from Fig. 5 is equal to the curve "AP 5" in the corresponding diagrams of the joint and motor torques.

nisms. Therefore, only the positive components of the power trajectories, $P_+(t)$, are used to compute the total consumed energy $E = \int P_+(t)\mathrm{d}t$, given in Table V.

1. Simulation: The designed PD-controlled motor trajectories for each joint consist of oscillations between two angles corresponding to a bent and stretched leg to simulate the synchronous flexion and subsequent extension in each step with a cycle time of 0.4 s. In all simulation runs the hip joint is actuated by a b-SEA with torsional stiffness 280 $^{\mathrm{Nm}}/_{\mathrm{rad}}$ to move between 3° and 20°. Note also that the P and D controller gains are the same for all simulation runs to avoid variations in the results due to the gains (listed in Table IV). The knee and ankle joints are only actuated by the extending u-SEAs. Estimation of the corresponding motor angles θ was performed by computing the equilibrium length of the tendons for the desired joint angles. In this first run the ground contact is eliminated to avoid any interferences of the results through the contact dynamics. The range of interesting spring stiffnesses were selected based on human experiment data, as described in [15], and was also validated in experiments. An overview of the selected rest lengths, attachment points and spring stiffnesses for all structures in each run is given in Table III.

TABLE III

SIMULATION STUDY: LEG CONFIGURATION.

Exp. No.	Joint	Muscle	Stiffness [N/mm]	Attachment [number]	Rest length [deg]
1	Knee	VAS	15	5	-60
	Ankle	SOL	8	4	3
2 (3)	Knee	VAS	15	5	-60
		PL	8	1 (3)	-60
	Ankle	SOL	8	4	3
		TA	3	3	3
4	Knee	VAS	15	5	-60
		PL	8	3	-60
		GAS	8	1	-45
	Ankle			1	-10
		SOL	8	4	3
		TA	3	3	3

As expected, the hip motor activity leads to the desired joint behavior oscillating between the flexed and extended position due to the bidirectional actuation. The knee and ankle motors, however, achieve an actuation in only one direction. Both joints are extended by the motors, but the movements backwards to the flexing positions do not occur correctly, particularly in the ankle joints. In the knee joints we can recognize a periodic pattern, but with an offset of almost 30° close to quite extended positions. The knee joints are actually overextending. Note that mechanical joint limits were removed on purpose to detect among others

Preprint of paper which appeared in the Proceedings of the 2012 IEEE/RSJ International Conference on Intelligent Robots and Systems, pp.4243-4250.

such effects. Apparently, extending and releasing the tendons are not sufficient to retain the desired periodic patterns, particularly in the presence of friction, which is currently only considered in motor and joint for the u-SEAs. The most energy is consumed for the actuation of the knee joint which is due to the high motor velocity, followed by the hip joint also due to the high motor velocity. Details are provided in Table V. As flexion and extension do not occur correctly, for the time being we do not introduce ground contact.

2. Simulation: Instead, the antagonistic structures PL and TA are added to the knee and ankle joint. The desired periodic patterns in knee and ankle joint become now realizable, but at the price of higher motor torques due to the opposing torques of the antagonists on the motors. This in turn results in higher overall energy consumption by around 44%, from 89.33 J to 128.63 J. Interestingly, the energy required for the hip motor is increased by 62%, although the introduced structures do not cross the hip joint. As Kuo noticed in [19], the torques induced do not necessarily only affect directly the joint the structure is crossing, but can also cause other joints to move. The increased energy is thus due to higher external torques acting on the hip.

3. Simulation: After the realization of some kind of simultaneous flexion and extension of all leg joints we introduce the ground contact to see if hopping can be achieved. To accommodate for the ground contact, the attachment point of PL was changed from number 1 to 3. The ground contact supports the flexion of ankle and knee joints. Therefore, the PL structure can react slower than in the previous run. All other settings were not changed to prevent complicating the access to insights. One obvious difference now is the full flexion of the ankle joints due to the ground contact. Although the parameter settings were not tuned to achieve optimal performance, the knee and ankle joints are quite synchronously flexed and extended. From the animations we can recognize clear flight phases and dynamic ground clearances. The average duty factor amounts to 0.3, i.e. ground contact takes place only during 30% of the total cycle time. The average ground clearance is 13 cm. Further, the ground reaction forces (GRF) have the typical vertical single-humped patterns known from humans during hopping and running. The energy required by the hip and knee motors are reduced by 33% and 21%, respectively. Only the ankle motors need more power to track the output joint trajectory due to the external torques induced by the ground contact. In total, the consumed energy is decreased by 23% to 99.68 J confirming the positive supporting impact by the ground.

4. Simulation: The above run is repeated with a GAS structure in each leg to analyze its impacts. Several slight changes in a positive direction can be observed. First, the GRF patterns are smoother. Second, the computed average duty factor decreased from 0.3 to 0.29, i.e. flight phases are increased. The ground clearances in average amount to 14 cm. Also, it can be noted that the ground contact occurs more regularly and there is less variation in flight phase and ground clearance compared to the previous simulation. Besides, the flexion of the ankle joints, intensified by the ground contact already in *3. Simulation*, is now reduced to the necessary degree. Interestingly, these positive effects are achieved without even optimizing the design parameters for the best possible results. Another effect, that is not consistent with biomechanical findings, can be detected. While the torques generated by the GAS structure on the ankle joint are negative and thus "cooperating" with the motor for the ankle extension, the torques on the knee joint by GAS are positive, aside from a small negative curve at the beginning of the hopping motion. The reason why we observe this during the simulated motion is that the force line of ${}^{\mathrm{Kne}}\boldsymbol{F}$ crosses the knee joint depending on the location of its attachment on the knee side in the x-y-plane and as well the knee angle. Although positive GAS torques support the knee motor, the energy consumption slightly increases, as the GAS activity also increases the PL torques which in turn lead to higher VAS torques. Optimized settings could help to optimally coordinate the various actions.

TABLE IV

SIMULATION STUDY: MOTOR CONTROLLER GAINS

P-gain hip b-SEA $k_p = 200$	D-gain hip b-SEA $k_d = 50$
P-gain knee VAS $k_p = 30$	D-gain knee VAS $k_d = 8$
P-gain ankle SOL $k_p = 30$	D-gain ankle SOL $k_d = 4$

TABLE V

SIMULATION STUDY: ENERGY CONSUMPTION

Exp.	**Hip**	**Knee**	**Ankle**	**Leg**
No.	E [J]	E [J]	E [J]	$\mathbf{\Sigma E}$ [J]
1	39.0458	43.9008	6.3861	89.3327
2	63.5794	58.5832	6.4685	128.6311
3	42.8959	46.5979	10.1847	99.6787
4	54.2539	49.5667	8.4033	112.2286

VI. DISCUSSION

The presented models of all actuator types allowed us to capture their dynamics during vertical hopping motions and to draw several first conclusions. The b-SEA in the hip can be considered as a conventional SEA, because it actuates both directions. More interesting for us were the tendon-based structures spanning one or two joints. It became clear, that during hopping the monoarticular structures cannot fulfill their designated roles without their counteracting structures. Thus, they should be deployed in pairs, requiring two tendons with built-in extension springs but only one motor. The flexion then occurs passively at an activation time instant depending on the set rest length. Compared to the actuation with a b-SEA, this is a more energy-efficient way of moving a joint in both directions. The use of the biarticular structure GAS resulted in smoother ground contact patterns, longer flight phases and larger ground clearances without even optimized structure settings yet. As it takes on the role of ankle extension, it is thinkable to omit the ankle motor to enhance energy savings.

Furthermore, such models and the corresponding joint torques analyses enable to derive design guidelines which do not have to be consistent with biomechanical findings for human legs. As observed during the *4. Simulation*, the GAS also produces positive torques on the knee joint, interestingly

"cooperating" with the motor for the knee extension. This is not in accordance with human biomechanics where the GAS is known to support the knee flexion. Apparently the attachment on the knee side can be adjusted such that the force line never crosses the knee joint and in this way always acts in conformity with the biomechanial insights only as knee flexor and ankle extensor. But regarding energy consumption it is imaginable to benefit from this observed effect. If the settings are well tuned, the motor for the knee extension must do less work when additionally supported by the GAS structure. It is even thinkable to completely omit the knee motor for the extension, as for instance also suggested in [20].

But such reasonings are not possible without the mathematical approach presented in this paper. To validate the proposed models, we extensively investigated various characteristic curves to check the plausibility of the results which due to limited space had to be shortened (cf. Section IV). Additionally, we applied another method computing the Jacobian matrices to determine the acting torques and obtained consistent results. The presented mathematical approach is not limited to the specific construction of the BioBiped robots. The models can be used in MBS dynamics simulations to study the specific roles of muscles mentioned in biomechanical literature and their optimal layout and parameters. As elucidated in Section IV, the design space provides for different setting opportunities: rest lengths, attachment points, and spring stiffnesses, aside from structural placings of the fixed and moving fixation points in general. It is a great challenge to overview these "regulating screws" and to define guidelines for their beneficial use to affect bandwidth, response delay, joint stiffness, and the overall observed compliance of the whole system. The purpose of this paper is to provide the basis for design and performance studies by MBS dynamics simulations in sufficient detail so that the results can be carried over to real robots.

VII. CONCLUSIONS AND OUTLOOK

In this paper, detailed mathematical models have been derived from the classical mechanical principle of virtual displacement and work for the active and passive, mono- and biarticular elastic structures of tendon-driven, series elastically actuated, musculoskeletal robots. This mathematical approach is highly important as it provides a reliable basis to study effects like variation of the motor and joint torques caused by the action of the actuators and passive structures as well as external influences on the motion performance of a musculoskeletal robot. Such detailed analyses are essential to understand also how to tackle the arising problem of intelligent motion control and to reduce the amount of energy that has to be supplied by the motors. In preliminary evaluation we could observe positive effects of the passive mono- and biarticular structures and confirm previous statements from biomechanists regarding their potential of saving energy. The range of future works is huge. The presented equations enable the development of a suitable framework to investigate more in-depth the design space of the actuator types by varying the many tuning parameters to determine the operation ranges. Equally important, it has been made possible to analyze which of the many possible actuation structures are actually essential to achieve fast dynamic motions.

REFERENCES

[1] R. V. Ham *et al.*, "Compliant actuator designs," *IEEE Robot. Automat. Mag.*, vol. 16, no. 3, pp. 81–94, 2009.
[2] G. A. Pratt and M. M. Williamson, "Series elastic actuators," in *IEEE Int. Workshop Intell. Robot. Syst.*, 1995, pp. 399–406.
[3] G. Palli *et al.*, "Tendon-based transmission systems for robotic devices: Models and control algorithms," in *Proc. IEEE ICRA*, 2009, pp. 4063–4068.
[4] K. W. Hollander and T. G. Sugar, "Powered human gait assistance," *InTech*, 2007.
[5] J. F. Veneman *et al.*, "A series elastic- and bowden-cable-based actuation system for use as torque actuator in exoskeleton-type robots," *IJRR*, vol. 25, no. 3, pp. 261–281, 2006.
[6] H. G. Marques *et al.*, "Ecce1: The first of a series of anthropomimetic musculoskeletal upper torsos," in *Proc. IEEE-RAS HUMANOIDS*, 2010, pp. 391–396.
[7] D. Hobbelen *et al.*, "System overview of bipedal robots Flame and TUlip: tailor-made for Limit Cycle Walking," in *Proc. IEEE/RSJ IROS*, 2008, pp. 2486–2491.
[8] K. Hosoda *et al.*, "Pneumatic-driven jumping robot with anthropomorphic muscular skeleton structure," *Autonomous Robots*, vol. 28, no. 3, pp. 307–316, 2010.
[9] B. Verrelst *et al.*, "The pneumatic biped "Lucy" actuated with pleated pneumatic artificial muscles," *Autonomous Robots*, vol. 18, no. 2, pp. 201–213, 2005.
[10] R. Niiyama *et al.*, "Mowgli: A bipedal jumping and landing robot with an artificial musculoskeletal system," in *Proc. IEEE ICRA*, 2007, pp. 2546–2551.
[11] G. J. van Ingen Schenau *et al.*, "The unique action of bi-articular muscles in complex movements," *J. Anatomy*, vol. 155, pp. 1–5, 1987.
[12] R. Jacobs *et al.*, "Mechanical output from individual muscles during explosive leg extensions: The role of biarticular muscles," *J. Biomechanics*, vol. 29, no. 4, pp. 513–523, April 1996.
[13] H. Kino *et al.*, "Basic study of biarticular muscle's effect on muscular internal force control based on physiological hypotheses," in *Proc. IEEE ICRA*, 2009, pp. 4195–4200.
[14] B. Lim *et al.*, "Optimal jumps for biarticular legged robots," in *Proc. IEEE ICRA*, 2008, pp. 226–231.
[15] K. Radkhah *et al.*, "Concept and design of the BioBiped1 robot for human-like walking and running," *Int. J. Humanoid Robot.*, vol. 8, no. 3, pp. 439–458, 2011.
[16] Biobiped project website. [Online]. Available: www.biobiped.de
[17] L. Grègoire *et al.*, "Role of mono- and biarticular muscles in explosive movements," *Int. J. Sports Medicine*, vol. 5, pp. 301–305, 1984.
[18] T. Lens *et al.*, "Simulation of dynamics and realistic contact forces for manipulators and legged robots with high joint elasticity," in *Proc. Int. Conf. Advanced Robot.*, 2011, pp. 34–41.
[19] A. D. Kuo, "The action of two-joint muscles: The legacy of W. P. Lombard." in *Classics in Movement Science*, Human Kinetics ed., M. L. Latash and V. M. Zatsiorsky, Eds. Champaign, 2001, pp. 289–316.
[20] K. Endo and H. Herr, "A model of muscle-tendon function in human walking," in *Proc. IEEE ICRA*, 2009, pp. 1909–1915.